

# Myocardial Iodine-123-Metaiodobenzylguanidine Images and Autonomic Nerve Activity in Normal Subjects

Takakazu Morozumi, Hideo Kusuoka, Kazuki Fukuchi, Akihiro Tani, Toshiisa Uehara, Shin'ichi Matsuda, Eiichiro Tsujimura, Yasushi Ito, Masatsugu Hori, Takenobu Kamada and Tsunehiko Nishimura

The First Department of Medicine, Division of Tracer Kinetics, Biomedical Research Center, Osaka University Medical School, Suita, Osaka; and Department of Internal Medicine, Osaka Koseinenkin Hospital, Fukushima, Osaka

We studied the relationship between myocardial [ $^{123}\text{I}$ ]metaiodobenzylguanidine (MIBG) uptake and autonomic nerve activity in normal subjects. **Methods:** MIBG scintigraphy and power spectral analysis (PSA) of heart rate variability were performed simultaneously in 15 normal subjects. Anterior planar images and SPECT images were taken at five and two points after the injection of [ $^{123}\text{I}$ ]MIBG, respectively. In 10 of 15 subjects,  $^{201}\text{Tl}$  myocardial SPECT was performed immediately after MIBG scintigraphy. **Results:** The heart/upper mediastinum MIBG uptake ratio in the planar image obtained at 240 min ( $r = 0.64$ ,  $p < 0.01$ ) and the washout rate of MIBG in the heart between 15 min and 240 min ( $r = 0.51$ ,  $p < 0.05$ ) showed significant correlation with the percentage of low frequency component of PSA (percent LF), an index of sympathetic nerve activity. Regional MIBG uptake in the inferior wall normalized by individual maximal uptake among all pixels was significantly correlated with the high frequency component of PSA, an index of parasympathetic nerve activity ( $r = -0.58$ ,  $p < 0.05$ ) and with mean R-R interval in a resting ECG ( $r = -0.82$ ,  $p < 0.001$ ) but did not correlate with percent LF, percent uptake of  $^{201}\text{Tl}$  in the inferior wall or the liver/heart uptake ratio. **Conclusion:** These results indicate that myocardial MIBG uptake correlates with sympathetic nerve activity in normal subjects. Our data indicate that heterogeneous MIBG distribution in the left ventricle is a physiologic rather than artifactual phenomenon and may be related to vagal tone rather than sympathetic nerve activity.

**Key Words:** iodine-123-MIBG; sympathetic nerve activity; parasympathetic nerve activity

**J Nucl Med 1997; 38:49-52**

Abnormalities in the myocardial uptake of [ $^{123}\text{I}$ ]metaiodobenzylguanidine (MIBG) have been reported in various cardiac diseases (1-8). Three possible mechanisms for the abnormal uptake have been suggested (6,8). They include: damage to sympathetic nerve endings including dysfunction of norepinephrine reuptake, reduced density of myocardial sympathetic nerve endings resulting in complete or partial denervation and augmented sympathetic nerve activity. Furthermore, the myocardial MIBG distribution in the left ventricle (LV) has shown to be inhomogeneous in some patients (9,10). Three mechanisms were also proposed for differences in MIBG uptake between the anterior and inferior myocardial walls (11). They include: physiologic inhomogeneity of innervation or autonomic activity, attenuation based on the depth of the source or diaphragmatic attenuation and artifact in the image reconstruction of SPECT caused by high radionuclide counts in the liver.

Received Nov. 28, 1995; revision accepted May 1, 1996.

For correspondence contact: Hideo Kusuoka, MD, PhD, Division of Tracer Kinetics, Biomedical Research Center, Osaka University Medical School, Suita, Osaka 565, Japan.

For reprints contact: Tsunehiko Nishimura, MD, PhD, Division of Tracer Kinetics, Biomedical Research Center, Osaka University Medical School, Suita, Osaka 565, Japan.

In contrast, power spectral analysis (PSA) of heart rate variability is well-established as a clinical estimate of autonomic nerve function (12,13). To clarify the relationship between myocardial MIBG images and autonomic nerve activity, and to elucidate the major mechanism for heterogeneous MIBG distribution in the LV, we performed MIBG scintigraphy and PSA simultaneously in 15 healthy subjects.

## MATERIALS AND METHODS

Fifteen normal male volunteers (age 20-60 yr, mean age  $32 \pm 10$  yr) who had no significant medical history were studied. None of the subjects took any medications known to affect autonomic nerve function. Physical examination and an electrocardiogram at rest performed at the entry into the study revealed no abnormalities in any subject. All volunteers were enrolled in the protocol which was approved by the Institutional Committee of Osaka University Hospital for Clinical Research.

### MIBG Scintigraphy

MIBG scintigraphy was performed at rest. Anterior planar images ( $256 \times 256$  matrix) were acquired over 5 min at five points, i.e., 15, 60, 110, 180 and 240 min after the intravenous injection of MIBG (111 MBq). SPECT images ( $64 \times 64$  matrix) of MIBG were obtained twice, i.e., 25 and 250 min after the injection, using a rotating, three-headed gamma camera, equipped with a low-energy collimator ( $120^\circ$  rotation). Each rotational step took 1 min. A total of 20 steps were performed over 20 min. In 10 of 15 subjects,  $^{201}\text{Tl}$  myocardial SPECT was performed 10 min after the injection of  $^{201}\text{Tl}$  (111 MBq) immediately after the completion of a series of MIBG scintigraphy. All SPECT data were acquired with three energy windows for scatter correction (14,15).

### Images Analysis

For the analysis of MIBG kinetics, four regions of interest (ROIs) were defined on planar images [upper mediastinum, right lung, liver and heart (Fig. 1A)]. The mean radionuclide count per pixel in each ROI was calculated. Two indices of myocardial MIBG accumulation in the planar images were used in the analysis (16-18). The first index was the ratio of MIBG uptake in the heart to that in the upper mediastinum (H/M). The other was the decreased counting rate in the heart normalized by the count at 15 min after injection (percent washout rate). The liver/heart MIBG uptake ratio (Li/H) was also calculated to assess the relationship between MIBG uptake in the liver and in the heart.

For SPECT images analysis, polar maps of relative tracer activity were generated from short-axis tomograms using circumferential profile analysis (19) with a maximal search algorithm (20). Briefly, maximum count circumferential profiles, in which each point represented the maximum counts per pixel along a radius extending from the center of the left ventricle to the limit of the radius of search, were generated from each short-axis tomo-

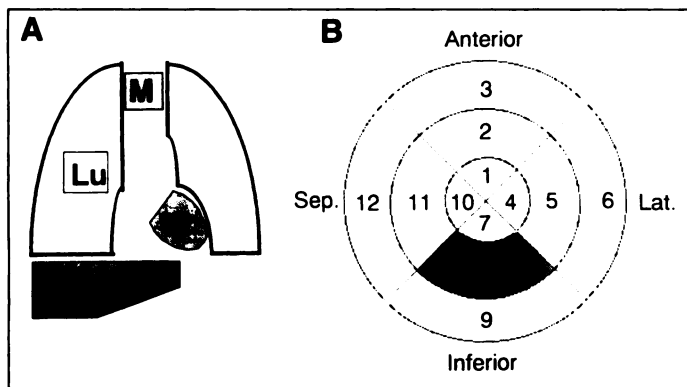


**FIGURE 1.** ROIs in planar images and segmentation in polar maps. (A) Locations of ROIs set in an anterior planar image. M, Lu, Li and H indicate ROIs in the upper mediastinum ( $12 \times 12$  pixels, square), the midportion of the right lung ( $12 \times 12$  pixels, square), liver ( $12 \times 12$  pixels, square) and heart (drawn by free hand), respectively. (B) Segments in a polar map. The mean percent uptake in the inferior wall (percent U) is defined as that in segment eight (midportion of the inferior wall).

gram. Each set of profiles was normalized so that the maximum pixel value in all slices was set to 100. The count profiles from all tomograms were plotted onto a polar map. Then, the LV was divided into 12 segments (Fig. 1B), and the uptake per pixel in each segment was normalized by the individual maximal value among all pixels. All SPECT data were corrected to remove the scatter photons using the three energy-window method (14,15). Three subjects were eliminated from the study. In two of these, delayed images could not be reconstructed because of low myocardial counts, and in the remaining subject high accumulation in the liver precluded analysis of the heart. SPECT data of the remaining 12 subjects were used in the final analysis. The regional washout rate was calculated from the early and delayed SPECT images.

#### Power Spectral Analysis of Heart Rate Variability

To evaluate autonomic nerve activity, PSA of heart rate variability was performed simultaneously with the acquisition of the 15-min image using the autoregression method (12). The percentage of low frequency components in the power spectral density [0.05–0.15 cycle/beat (c/b)], percent LF and the power spectral density of high-frequency (HF) component (0.15–0.4 c/b) were calculated. The percent LF was used as the index of sympathetic nerve activity whereas HF has been used as the index of parasympathetic nerve activity (13).

#### Measurement of Plasma Catecholamine Level

In 10 of 15 subjects, blood samples were collected at the end of the acquisition of the initial image data (15 min). Plasma concentrations of norepinephrine and epinephrine were measured by high-performance liquid chromatography (HPLC).

#### Statistical Analysis

All data are expressed as mean  $\pm$  s.d. Regression analysis, paired t-test and analysis of variance with Bonferroni's method were used where appropriate. Probability ( $p$ )  $< 0.05$  was considered statistically significant.

### RESULTS

#### Myocardial Kinetics of MIBG in Normal Subjects

The mean radionuclide count per pixel in each ROI during the 4 hr after the injection are displayed graphically in Figure 2. All count data were corrected by the injected dose for between individual comparison. The MIBG uptake per pixel was highest in the liver, and higher in the heart than in the lung (Fig. 2A). MIBG accumulation in the liver reached peak levels at 60 min, which was delayed when compared with the heart and lung. The

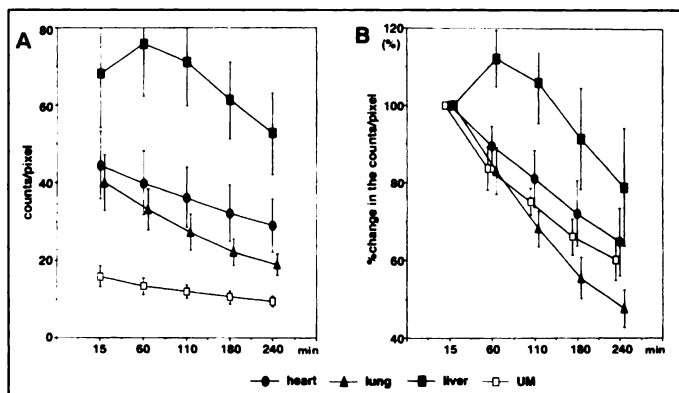


**FIGURE 2.** Changes of MIBG in each ROI in normal volunteers. (A, B) Mean radionuclide counts per pixel in each ROI and percent change of mean counts in each ROI from the 15-min baseline, respectively. Counts in each ROI were corrected by the injected dose. Note that activity in the liver is highest. Error bars represent s.d.

MIBG washout rate in the lung was the highest among the three organs (Fig. 2B).

The H/M ratio increased after 60 min ( $2.80 \pm 0.25$  at 15 min,  $3.00 \pm 0.35$  at 60 min,  $3.03 \pm 0.40$  at 110 min,  $3.07 \pm 0.49$  at 180 min and  $3.02 \pm 0.47$  at 240 min) but not significantly. However, due to the faster MIBG washout in the lung, the myocardial MIBG image was more visible in the delayed images. Only 2 of 15 subjects had a less visible myocardial delayed image compared with early images. We, therefore, recommend that 240-min images be used to assess myocardial MIBG distribution.

The myocardial MIBG washout rate for 240 min (percent washout rate) in 15 normal subjects was  $35.1\% \pm 8.7\%$  without decay correction and  $20.7\% \pm 10.7\%$  with correction by half-life time.

#### Relation between MIBG Kinetics and Sympathetic Nerve Activity

No subject had abnormal plasma catecholamine levels. The H/M ratio obtained from the 240-min images and the percent washout rate were significantly correlated with percent LF ( $r = 0.64$ ,  $p < 0.05$  for H/M, Fig. 3A;  $r = 0.51$ ,  $p < 0.05$  for percent washout rate, Fig. 3B).

#### Segmental Distribution of Myocardial MIBG Uptake

Regional percent uptake in each segment is shown in Table 1. The uptake in segments one to six (anterior and lateral walls of the LV) were relatively higher than those in segments 7 to 12. The percent uptake in segment 12 showed the lowest value among all segments, but this was caused by an artifact in the generation of the polar maps. To clarify the major mechanism

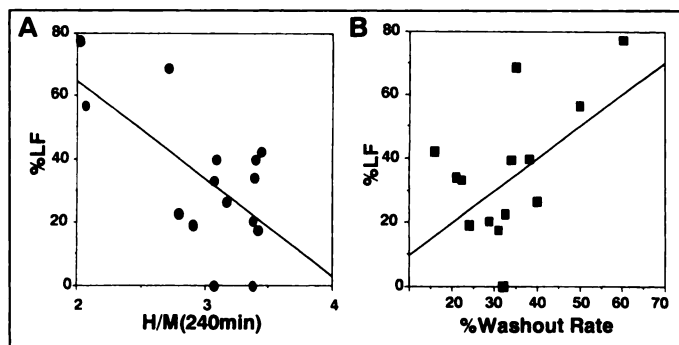


**FIGURE 3.** Correlation between the H/M ratio and washout rate derived from MIBG images and sympathetic nerve activity (percent LF) in normal subjects. The H/M ratio was obtained from delayed (240-min) images.

**TABLE 1**  
Segmental MIBG Uptake on Early and Delayed Images and the Washout Rate

Segment no.	Uptake (%)		Washout Rate (%)
	Early	Delayed	
1	84.6 ± 4.5*	87.4 ± 3.1*	13.5 ± 6.9
2	88.5 ± 4.1*	90.9 ± 4.5*	14.8 ± 6.4
3	82.9 ± 6.0*	86.0 ± 4.8*	13.5 ± 9.0
4	84.0 ± 4.9*	83.7 ± 4.7*	16.7 ± 7.6
5	87.5 ± 3.0*	87.6 ± 2.7*	16.5 ± 9.0
6	87.5 ± 4.2*	87.3 ± 5.0*	16.7 ± 9.5
7	75.1 ± 7.2	77.5 ± 5.8	13.9 ± 10.4
8	74.0 ± 7.4	74.1 ± 4.5	16.0 ± 10.8
9	70.0 ± 7.6*	68.6 ± 5.3*	18.2 ± 10.2*
10	75.8 ± 6.5	80.7 ± 7.5	11.8 ± 9.3
11	74.5 ± 7.5	78.5 ± 7.6	12.4 ± 8.5
12	65.2 ± 6.4*	65.8 ± 6.3*	15.8 ± 11.4

\*p < 0.05 vs. the value in segment 8 by ANOVA with Bonferroni's method.

for heterogeneous MIBG distribution in the LV, the regional percent uptake in segment 8 (percent U) was correlated with several other factors. Among the factors indicating autonomic nerve activity, HF, i.e., the index of parasympathetic nerve activity ( $r = -0.58$ ,  $p < 0.05$ ; Fig. 4A) and the mean R-R interval of the resting ECG ( $r = 0.82$ ,  $p < 0.001$ ; Fig. 4C) showed significant negative correlation with percent U whereas

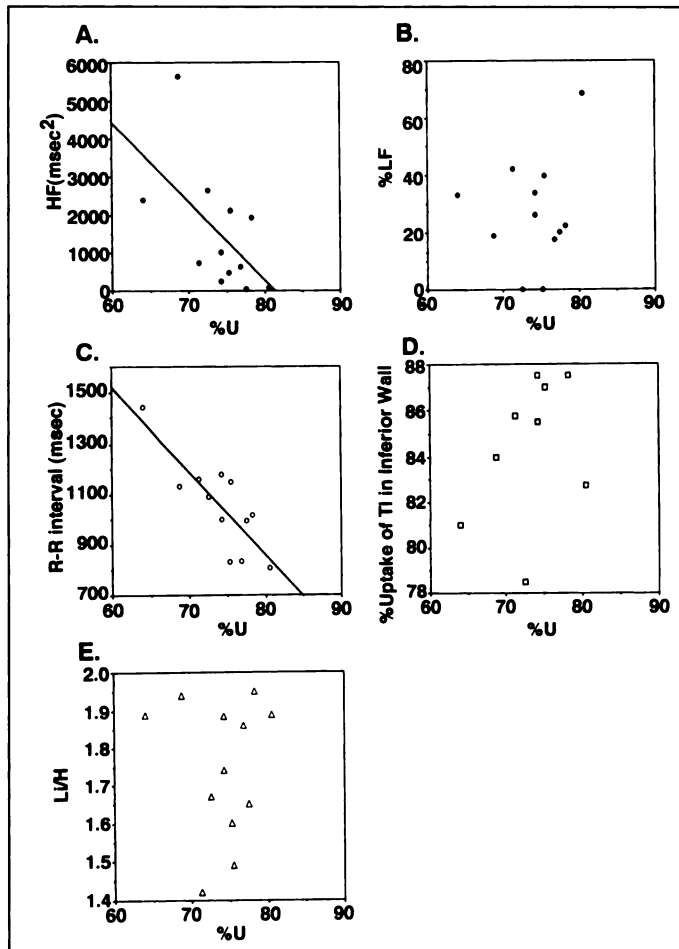


**FIGURE 4.** Correlation between regional percent uptake of MIBG in the inferior wall (percent U) and various parameters. (A) HF in PSA. (B) Percent LF in PSA. (C) Mean R-R interval in resting ECG. (D) Percent uptake of  $^{201}\text{Tl}$  in inferior wall. (E) The liver/heart uptake ratio.

percent LF failed to show a correlation with percent U (Fig. 4B). Regional percent uptake at the same segment (# 8) of  $^{201}\text{Tl}$  myocardial SPECT failed to correlate with percent U (Fig. 4D), indicating that body attenuation of radionuclide counts is not the mechanism for the LV heterogeneity. Furthermore, Li/H did not correlate with percent U (Fig. 4E), suggesting that liver uptake does not play a role in the LV heterogeneity. In contrast, percent uptake in other than inferior wall (i.e., segment 2, 5 or 11) showed no significant correlation with HF, percent LF or R-R intervals (data not shown).

## DISCUSSION

Iodine-123-MIBG myocardial scintigraphy has been used widely in patients with ischemic heart disease (5), congestive heart failure (6), valvular disease (7) and cardiomyopathy (23). It is, however, necessary to understand the normal ranges of indices used in the evaluation of MIBG myocardial images. Many regional MIBG defects are detected in the septum or inferoposterior wall (7,9-11,24). It was also reported that regional MIBG uptake in the septum, posterior wall and inferior wall were lower than that in the anterior wall in normal persons (11).

### MIBG Kinetics in Normal Subjects

Our data indicates that washout is fastest in the lung and slowest in the liver; washout from the heart and the upper mediastinum are of intermediate range (Fig. 2B). The H/M ratio was almost constant over 240 min. This may be due to the fact that MIBG clears from nonspecific binding sites to the same degree in the mediastinum and myocardium. In most subjects, the MIBG cardiogram was most visible in the images at 240 min after injection, and we favor this delay to assess myocardial MIBG distribution. However, in 2 of 15 subjects, the MIBG cardiograms became less well-delineated with time, indicating a higher washout rate of myocardial MIBG compared with the other individuals. The data for these two patients were included in the analysis. The mechanism for these atypical MIBG images remains unknown.

Augmented sympathetic nerve activity is thought to reduce myocardial MIBG uptake and increase washout based on studies in patients with various heart disease (1,3,4,6,21,22) including congestive heart failure. Schofer et al. (17) reported that the myocardial compared with mediastinal MIBG activity ratio was significantly correlated with myocardial norepinephrine concentration and left ventricular ejection fraction in patients with idiopathic dilated cardiomyopathy. Our study suggests that myocardial MIBG uptake and its washout may be correlated with sympathetic nerve activity even in normal subjects.

### Mechanism for Heterogeneous MIBG Left Ventricular Uptake

Regional MIBG uptake in normal subjects was inhomogeneous and apparently lower in the septum and the inferoposterior wall than in the anterior or lateral walls, as reported previously (11). In contrast, examinations using PET with  $^{11}\text{C}$ -hydroxyephedrine and  $^{18}\text{F}$ -fluoro-dopamine (25,26) did not produce a heterogeneous distribution of myocardial uptake. Thus, the difference in distribution may be specific to MIBG. Three mechanisms have been proposed for the heterogeneous MIBG distribution. The first mechanism is physiologic variation in sympathetic innervation. Previous studies demonstrated that the anterior wall has predominantly sympathetic afferent innervation (27,28). In contrast, a recent study by Minisi et al. (29) have indicated that sympathetic afferent nerves were distributed equally to the inferoposterior and anterior walls in

dogs. Our study also showed that percent LF, the index of sympathetic nerve activity, did not correlate with percent U, an index of relative regional MIBG uptake in the inferoposterior wall. The second proposed mechanism is attenuation including that by diaphragm (11). Our study showed that the regional percent uptake of <sup>201</sup>Tl did not correlate with that of MIBG (percent U) in the same segment in the inferior wall.

Therefore, diaphragmatic attenuation plays little role in the heterogeneity of MIBG distribution in the LV. The third is the artifact in SPECT reconstruction caused by high uptake of MIBG in the liver; a previous phantom study demonstrated that the high count in the liver created artifactual defects (30). However, these regional defects are more frequently located in the inferior wall than in the anterior wall, even in the patients without liver congestion (9–11,24). Furthermore, the Li/H ratio did not correlate with percent U in this study. Therefore, we suggest that high hepatic uptake could create some artifactual defects in the inferior wall, but all defects in this region cannot be explained by this mechanism alone.

Our study and other studies indicate that three possible mechanisms mentioned above are suspicious for heterogeneous MIBG uptake in myocardium. On the other hand, it has been demonstrated by experimental and clinical observations that vagal afferent distributes preferentially to the inferoposterior wall (31–33). Additionally, our study indicates that percent U correlated with HF in PSA and the mean R-R interval in the ECG, which are regulated predominantly by vagal tone at rest. It is recognized that vagal tone can directly affect sympathetic nerve function through both muscarinic receptors existing at sympathetic nerve terminals (varicosities) and innervation of sympathetic nerve ganglions by parasympathetic nerve fibers (34,35). Coupled with these observations, it is strongly suggested that the heterogeneous MIBG distribution in the LV is caused by the depressor reflex mediated by the parasympathetic nerve fibers predominantly located in the inferoposterior wall. The real mechanism for the heterogeneous MIBG uptake is still not clear, but it should be noted that the heterogeneity is a physiological phenomenon, not an artifact.

## CONCLUSION

To clarify the relationship between myocardial MIBG images and autonomic nerve activity, we performed MIBG scintigraphy and PSA simultaneously in 15 healthy subjects. For the evaluation of [<sup>123</sup>I]MIBG uptake in myocardium, delayed images obtained 240 min after the injection were used because the MIBG cardiograms became progressively more distinct with time. Quantitative indices of myocardial MIBG uptake in planar images (H/M, percent washout rate) significantly correlated to percent LF, an index of sympathetic nerve activity in PSA, indicating that myocardial MIBG kinetics may be correlated with autonomic nerve activity in normal subjects. In addition, heterogeneous MIBG distribution in the LV is a physiologic phenomenon and may be related to vagal tone rather than sympathetic nerve activity.

## REFERENCES

- Muller KD, Jakob H, Neuzner J, Grebe SF, Schlepfer M, Pitschner HF. Iodine-123-metaiodobenzylguanidine scintigraphy in the detection of irregular regional sympathetic innervation in long QT syndrome. *Eur Heart J* 1993;14:316–325.
- Mantysaari M, Kuikka J, Mustonen J, et al. Noninvasive detection of cardiac sympathetic nervous dysfunction in diabetic patients using [<sup>123</sup>I]metaiodobenzylguanidine. *Diabetes* 1992;41:1069–1075.
- Fujiwara Y, Hamada M, Shigematsu Y, Sumimoto T, Hamamoto K, Hiwada K. Scintigraphic assessment of cardiac adrenergic innervation in patients with essential hypertension. *J Cardiovasc Pharmacol* 1991;17(suppl):S148–S150.
- Wakasugi S, Wada A, Hasegawa Y, Nakano S, Shibata N. Detection of abnormal

- cardiac neuron activity in adriamycin-induced cardiomyopathy with iodine-123-metaiodobenzylguanidine. *J Nucl Med* 1992;33:208–214.
- Dae MW, Herre JM, O'Connell JW, Botvinick EH, Newman D, Munoz L. Scintigraphic assessment of sympathetic innervation after transmural versus nontransmural myocardial infarction. *J Am Coll Cardiol* 1991;17:1416–1423.
- Glowniak JV, Turner FE, Gray LL, Palac RT, Lagunas-Solar MC, Woodward WR. Iodine-123-metaiodobenzylguanidine imaging of the heart in idiopathic congestive cardiomyopathy and cardiac transplants. *J Nucl Med* 1989;30:1182–1191.
- Faget D, Wolf J, Vanzetto G, et al. Myocardial uptake of metaiodobenzylguanidine in patients with left ventricular hypertrophy secondary to valvular aortic stenosis. *J Nucl Med* 1993;34:57–60.
- Henderson EB, Kaln LK, Corbett JR, et al. Abnormal <sup>123</sup>I-MIBG myocardial washout and distribution may reflect myocardial derangement in patients with congestive cardiomyopathy. *Circulation* 1988;78:1192–1199.
- Shakespeare CF, Page CJ, O'Doherty MJ, et al. Regional sympathetic innervation of the heart by means of metaiodobenzylguanidine imaging in silent ischemia. *Am Heart J* 1993;125:1614–1622.
- Gill JS, Hunter GJ, Gane J, Ward DE, Camm AJ. Asymmetry of cardiac [<sup>123</sup>I]metaiodobenzylguanidine scans in patients with ventricular tachycardia and "clinically normal" heart. *Br Heart J* 1993;69:6–13.
- Gill JS, Hunter GJ, Gane G, Camm AJ. Heterogeneity of the human myocardial sympathetic innervation: in vivo demonstration by iodine-123-labeled metaiodobenzylguanidine scintigraphy. *Am Heart J* 1993;126:390–398.
- Pagani M, Lombardi F, Guzzetti S, et al. Power spectral analysis of heart rate and arterial pressure variabilities as a marker of sympatho-vagal interaction in man and conscious dog. *Circ Res* 1986;59:178–193.
- Task force of the European Society of Cardiology and the North American Society of Pacing and Electrophysiology. Heart rate variability. Standards of measurement, physiological interpretation and clinical use. *Circulation* 1996;93:1043–1065.
- Ichihara T, Ogawa K, Motomura N, Kubo A, Hashimoto S. Compton scatter correction using triple-energy window method for single- and dual-isotope SPECT. *J Nucl Med* 1993;34:2216–2221.
- Ogawa K. Simulation study of triple-energy-window scatter correction in combined <sup>201</sup>Tl, <sup>99m</sup>Tc SPECT. *Ann Nucl Med* 1994;8:277–281.
- Sisson JC, Shapiro B, Meyers L, et al. Metaiodobenzylguanidine to map scintigraphically the adrenergic nervous system in man. *J Nucl Med* 1987;28:1625–1636.
- Schofer J, Spielmann R, Schuchert A, Weber K, Schluter M. Iodine-123-metaiodobenzylguanidine scintigraphy: a noninvasive method to demonstrate myocardial adrenergic nervous system disintegrity in patients with idiopathic dilated cardiomyopathy. *J Am Coll Cardiol* 1988;12:1252–1258.
- Merlet P, Valette H, Dubois-Rande J, et al. Prognostic value of cardiac metaiodobenzylguanidine imaging in patients with heart failure. *J Nucl Med* 1992;33:471–477.
- Burow RD, Pond M, Schafer AW, et al. "Circumferential profiles": a new method for computer analysis of thallium-201 myocardial perfusion images. *J Nucl Med* 1979;20:771–777.
- Garcia E, van Train K, Maddahi J, et al. Quantification of rotational thallium-201 myocardial tomography. *J Nucl Med* 1985;26:17–26.
- Dae MW, O'Connell JW, Botvinick EH, et al. Scintigraphic assessment of regional cardiac adrenergic innervation. *Circulation* 1989;79:634–644.
- Sisson JC, Wieland DM, Sherman P, Mangner TJ, Tobes MC, Jacques S. Metaiodobenzylguanidine as an index of the adrenergic nervous system integrity and function. *J Nucl Med* 1987;28:1620–1624.
- Nakajima K, Bunko H, Taki J, et al. Quantitative analysis of <sup>123</sup>I-MIBG uptake in hypertrophic cardiomyopathy. *Am Heart J* 1990;119:1329–1337.
- Kleine RC, Swanson DP, Wieland DM, et al. Myocardial imaging in man with <sup>123</sup>I metaiodobenzylguanidine. *J Nucl Med* 1981;22:129–132.
- Goldstein DS, Chang PC, Eisenhofer G, et al. Positron emission tomographic imaging of cardiac sympathetic innervation and function. *Circulation* 1990;81:1606–1621.
- Schwaiger M, Kalff V, Rosenspire K, et al. Noninvasive evaluation of sympathetic nervous system in human heart by positron emission tomography. *Circulation* 1990;82:457–464.
- Geis WP, Kaye MP. Distribution of sympathetic fibers in the left ventricular epicardial plexus of the dog. *Circ Res* 1968;23:165–170.
- Pantridge JF. Autonomic disturbance at the onset of acute myocardial infarction. In: Schwartz P, Brown AM, Malliani A, Zanchetti A, eds. *Neural Mechanisms in Cardiac Arrhythmias*. New York: Raven Press; 1978:7–17.
- Minisi AJ, Thames MD. Distribution of left ventricular sympathetic afferent demonstrated by reflex responses to transmural myocardial ischemia and to intracoronary and epicardial bradykinin. *Circulation* 1993;87:240–246.
- Kobayashi H, Terada S, Kanaya S, et al. Artifactual defect of inferior myocardium on <sup>123</sup>I-metaiodobenzylguanidine myocardial SPECT: characteristic findings and preventive method on phantom study (in Japanese). *Kaku Igaku* 1994;31:359–366.
- Thames MD, Klopfeustein HS, Abboud FM, Mark AL, Walker JL. Preferential distribution of inhibitory cardiac receptors with vagal afferent to the inferoposterior wall of left ventricle activated during coronary occlusion in the dog. *Circ Res* 1978;43:512–519.
- Perez-Gomez F, Martin DR, Rey J, Garcia-Agnado A. Prinzmetal's angina: reflex cardiovascular response during episode of pain. *Br Heart J* 1979;42:81–87.
- Adgey AAJ, Geddes JS, Mulholland HC, Keegan DAJ, Pantridge JF. Incidence, significance and management of early bradyarrhythmia complicating acute myocardial infarction. *Lancet* 1968;2:1097–1101.
- Levy MN, Martin PJ. Neural control of the heart. In: Sperelakis N, ed. *Physiology and Pathophysiology of the Heart*. Boston: Martin Nijhoff; 1984:337–354.
- Braunwald E, Sonnenblick EH, Ross J. Mechanisms of cardiac contraction and relaxation. In: Braunwald E, ed. *Heart Disease*, 4th ed. Philadelphia: WB Saunders; 1992:351–392.